Enhancing the multiple harmonics by step-like cantilever

Feifei Gao, and Yin Zhang

Citation: AIP Advances **8**, 045108 (2018); doi: 10.1063/1.5023623
View online: https://doi.org/10.1063/1.5023623
View Table of Contents: http://aip.scitation.org/toc/adv/8/4
Published by the American Institute of Physics

Enhancing the multiple harmonics by step-like cantilever

Feifei Gao[1,2] and Yin Zhang[1,2,a]
[1]*State Key Laboratory of Nonlinear Mechanics, Institute of Mechanics, Chinese Academy of Sciences, Beijing 100190, China*
[2]*School of Engineering Science, University of Chinese Academy of Sciences, Beijing 100049, China*

(Received 26 January 2018; accepted 28 March 2018; published online 10 April 2018)

In atomic force microscopy (AFM), the higher modes are highly sensitive to the tip-sample interactions which generate many harmonics. When a higher harmonic is close to the natural frequency of a mode, the harmonic signal is enhanced by a resonance. The step-like cantilever is proposed as an effective design to enhance the higher harmonic signals. The natural frequencies are changed with the variations of the step-like cantilever sizes. By carefully designing the step-like cantilever, the first three modes can be simultaneously excited. A comprehensive map is provided as a guidance of selecting the appropriate geometric parameters.
https://doi.org/10.1063/1.5023623

The atomic force microscopy (AFM) is extensively used to investigate the material properties in nanoscale.[1] In tapping mode AFM, the peaks of the vibration spectrum are exhibited at integer multiples (higher harmonics) of the excitation frequency.[2] The higher harmonics are generated by the tip-sample interactions, which can be used to extract information on the material properties.[3–10] The enhanced resolution,[6,9] sensitivity[7] and better contrast[10,11] can be obtained in higher harmonics. For example, García *et al.*[9] demonstrated that bimodal AFM enables fast, accurate and angstrom-scale Young's modulus mapping on a wide range of materials in air and liquid. The trimodal AFM can be used as separate control "knobs" to simultaneously measure the topography, map compositional contrast and modulate sample indentation by the tip during tip-sample impact, respectively.[10] However, the higher harmonic signals are suppressed due to the rapid decay of frequency response curve of the uniform cantilever,[12] which may result in a small signal output that is even lower than the effective noise level. The vibration amplitudes of the higher harmonics are several orders of magnitude smaller than that of the fundamental component.[13] Therefore, the higher harmonic signals are inevitably lost.

The tip-sample interactions (F_{ts}) can be expanded into the following Fourier series: $F_{ts} = \sum_{n=0}^{\infty} \alpha_n \cos(n\omega t) + \beta_n \sin(n\omega t)$, ω is the driving frequency and $\sin(n\omega t)/\cos(n\omega t)$ is the harmonic, in which $n\omega$ is an integer multiple of ω. When the cantilever is driven by the fundamental frequency, the response of the cantilever at the nth harmonic will be dominated by the resonance of a mode whose natural frequency is an integer n multiple of the fundamental frequency.[5] Unfortunately, for a uniform cantilever, the natural frequencies of the higher modes are not integer multiples of the fundamental frequency. A great number of efforts have been made to enhance the higher harmonic signals. The higher harmonics are enhanced by simultaneously exciting the first two modes of a cantilever,[14] or by driving the cantilever around a submultiple of the fundamental frequency,[8,15] or by exciting the torsional modes in a torsional harmonic cantilever.[16] Besides excitation, the geometry of cantilever can also be modified to enhance its response. These modifications include fabricating the notch at the anti-node of the third mode,[12] introducing a paddle-like structure,[17–19] drilling holes with specific sizes and locations,[20–23] adding a concentrated mass at a specific location,[24] non-uniform width[25–29]

[a]Author to whom correspondence should be addressed. Electronic mail: zhangyin@lnm.imech.ac.cn (Y. Zhang).

and step cross section structure.[30–32] However, there are some deficiencies in those methods. For example, the concentrated-mass which is described by the Dirac delta function occupies a certain volume in practice.[24] The position of the hole, which is obtained from the finite element simulation, is difficult to be fabricated precisely in a practical application.[20,22,23]

In this study, a step-like cantilever design is proposed to enhance the higher harmonic signals. By simultaneously changing the length, width and thickness, the natural frequency of a mode can be tuned to coincide with a specific harmonic. The first three modes of a carefully designed step-like cantilever can be simultaneously excited. We provide a straightforward method of selecting the appropriate parameters of the step-like cantilever to tune the natural frequencies of the higher modes by a comprehensive map and a table.

In Fig. 1, the step-like cantilever consists of two parts: L_i, b_i and h_i (i = 1, 2) denote the length, width and thickness, respectively. The total length is $L = L_1 + L_2$. Subscript 1 denotes the parameters of the part with the fixed end, and subscript 2 denotes the parameters of the part with the free end.

The free vibration of a step-like cantilever is described by the following equations:[33–35]

$$\begin{cases} m_1 \frac{\partial^2 w_1}{\partial t^2}(x,t) + c_1 \frac{\partial w_1}{\partial t}(x,t) + E_1 I_1 \frac{\partial^4 w_1}{\partial x^4}(x,t) = 0, \ 0 \le x \le L_1, \\ m_2 \frac{\partial^2 w_2}{\partial t^2}(x,t) + c_2 \frac{\partial w_2}{\partial t}(x,t) + E_2 I_2 \frac{\partial^4 w_2}{\partial x^4}(x,t) = 0, \ L_1 \le x \le L. \end{cases} \tag{1}$$

Because of the step-like structure, the cantilever is divided into two parts: w_i, m_i, c_i and $E_i I_i$ (i = 1, 2) denote the cantilever deflection, mass per unit length, damping coefficient and flexural stiffness of the two parts, respectively. By introducing the following quantities $\xi = x/L$, $W_i = w_i/L$ (i = 1, 2) and $\tau = \sqrt{E_1 I_1 / m_1 L^4}\, t$, the following dimensionless equations are obtained:

$$\begin{cases} \frac{\partial^2 W_1}{\partial \tau^2} + \kappa_1 \frac{\partial W_1}{\partial \tau} + \frac{\partial^4 W_1}{\partial \xi^4} = 0, \quad 0 \le \xi \le \xi_o, \\ \gamma \frac{\partial^2 W_2}{\partial \tau^2} + \kappa_2 \frac{\partial W_2}{\partial \tau} + \chi \frac{\partial^4 W_2}{\partial \xi^4} = 0, \ \xi_o \le \xi \le 1. \end{cases} \tag{2}$$

Where $\xi_o = L_1/L$ is the length ratio of the first part to the total cantilever, which is also the location of the step as indicated in the coordinate system. Here $\gamma = m_2/m_1$ and $\chi = E_2 I_2 / E_1 I_1$ are the mass and flexural stiffness ratios for the two parts of the cantilever, respectively. And $\kappa_i = c_i \sqrt{L^4 / m_1 E_1 I_1}$ (i = 1, 2) is the dimensionless damping. For simplicity, $\rho_1 = \rho_2$ and $E_1 = E_2$ are assumed, hence, $\gamma = A_2/A_1$ and $\chi = I_2/I_1$. The ratios of ω_2/ω_1 and ω_3/ω_1 as the functions of ξ_o, γ and χ are obtained. The detailed computation procedures are given in the supplementary material.

The natural frequencies of the step-like cantilever and thus their ratios can be tuned with the variations of ξ_o, γ and χ. In Fig. 2(a), the ratio of ω_2/ω_1 as the function of γ and χ with $\xi_o = 0.5$ is presented, and the zoomed-in view of the boxed area is shown in Fig. 2(b). The ratio of ω_3/ω_1 as the function of γ and χ with $\xi_o = 0.5$ is presented in Fig. 2(c). As shown in Fig. 2, with γ and χ increasing, the ratios of ω_2/ω_1 and ω_3/ω_1 increase, except for the part ω_2/ω_1 around 3. In Fig. 2(b), when γ is less than 0.3, the ratio of ω_2/ω_1 is non-monotonic. With χ changing from

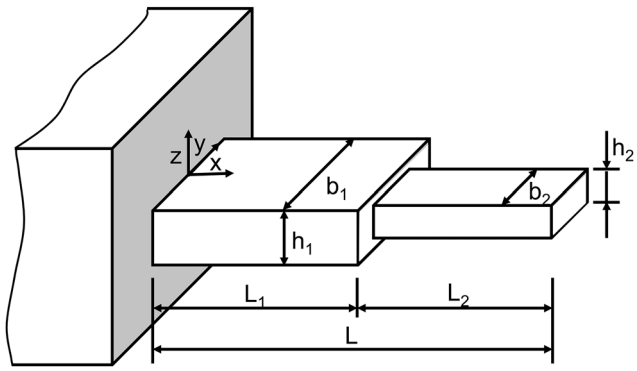

FIG. 1. Schematic diagram of the coordinate system and AFM cantilever dimensions.

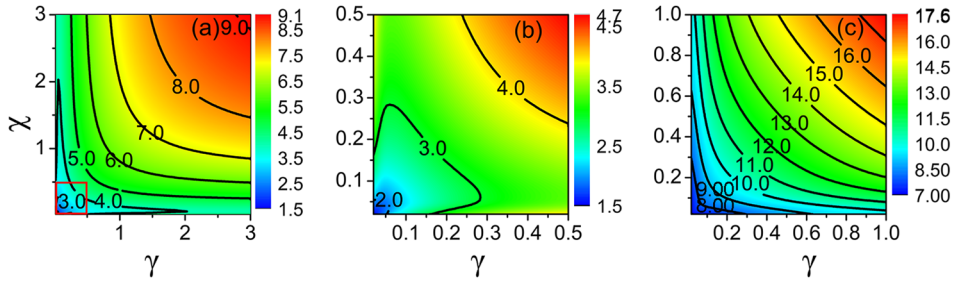

FIG. 2. The ratios of (a) ω_2/ω_1, (b) ω_2/ω_1 and (c) ω_3/ω_1 as the functions of γ and χ with $\xi_o = 0.5$. Here (b) is the zoomed-in view of the boxed area in (a).

0 to 0.5, the ratio of ω_2/ω_1 decreases firstly and then increases. When γ and χ remain constant, the ratio of ω_2/ω_1 shows a minimum at $\xi_o = 0.5$.[25] For a cantilever, when a mass is removed from the high mechanical stress region of the specific mode, the elastic energy and the natural frequency of the mode reduce.[12] The position of $\xi_o = 0.5$ is close to the highly curved region of the second mode. However, it is far from the highly curved region of the first mode. As a result, a smaller ratio of ω_2/ω_1 can be obtained at $\xi_o = 0.5$. When ξ_o increases from 0.5 to 1, the minimum integer multiple ratio of ω_2/ω_1 increases. For example, with the increasing of ξ_o, the minimum integer multiple ratio of ω_2/ω_1 increases from 2 to 5 in Fig. 3. When γ remains constant and χ changes from 0 to 0.5, the bending stiffness of the cantilever increases, and as a result the natural frequencies increase. However, the ratio of ω_2/ω_1 can be either increasing, decreasing or remaining constant. When the wider part is clamped, $\omega_2/\omega_1 < 6.27$ (the ratio value of a uniform cantilever). In comparison, when the narrower part is clamped, $\omega_2/\omega_1 > 6.27$. The results coincide with the results by Sadewasser *et al.*[28]

The integer n labels the curve that the natural frequency of the second mode (Fig. 3) or the natural frequency of the third mode (Fig. 4) equals to the nth harmonic. By interchanging the values of γ and χ, the figure with length ratio ξ_o can be regarded as the figure with length ratio $1 - \xi_o$ (Figs. 3

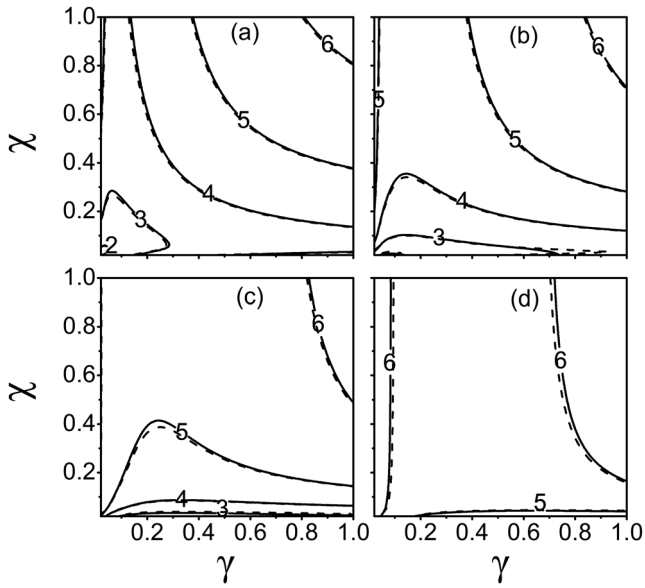

FIG. 3. Values of γ and χ which ensure an integer value of the ω_2/ω_1 ratio. The integers are labeled on the corresponding curves. (a) $\xi_o = 0.5$, (b) $\xi_o = 0.6$, (c) $\xi_o = 0.7$ and (d) $\xi_o = 0.8$. (The figure with length ratio ξ_o can also be regarded as the figure with length ratio $1 - \xi_o$ by interchanging the values of γ and χ). The solid line (—) and dashed line (- - -) are the corresponding curve of the undamped cantilever and damped cantilever, respectively.

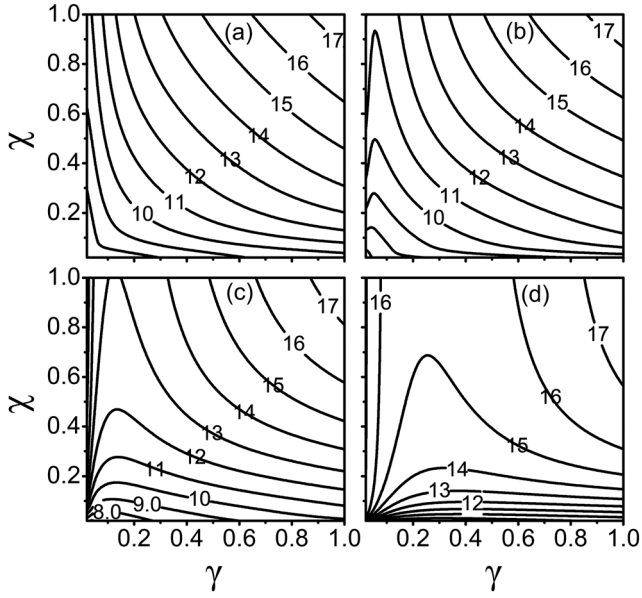

FIG. 4. Values of γ and χ which ensure an integer value of the ω_3/ω_1 ratio. The integers are labeled on the corresponding curves. (a) $\xi_o = 0.5$, (b) $\xi_o = 0.6$, (c) $\xi_o = 0.7$ and (d) $\xi_o = 0.8$. (The figure with length ratio ξ_o can also be regarded as the figure with length ratio $1 - \xi_o$ by interchanging the values of γ and χ).

and 4), because these two figures are symmetrical to the straight line of $\chi = \gamma$. The detailed proof is given in supplementary material. Therefore, the figures with $\xi_o = 0.2 \sim 0.5$ are omitted in Figs. 3 and 4. When the thickness of the two parts is with a significant difference, the bending of the thinner part dominates.[28] The ratios of ω_2/ω_1 are close to 6.27 with a smaller ξ_o. As shown in Fig. 3, when ξ_o varies from 0.5 to 0.8, the ratio of ω_2/ω_1 increases with the giving γ and χ. There is a similar tendency in Fig. 4. With the increasing of ξ_o, the influence of γ and χ becomes weaker, thus the frequencies of the step-like cantilever are close to those of a uniform cantilever.

When Fig. 4 is superimposed on top of the Fig. 3 of the same length ratio ξ_o, each of the intersection points defines a multiple harmonic cantilever. For example, letting Fig. 4(a) is superimposed on top of the Fig. 3(a). The first three modes of a multiple harmonic cantilever can be excited at the same time, which significantly enhances the higher harmonic signals. An application example is the trimodal AFM, which offers a way to locate and characterize the subsurface structures of the materials.[10] All intersection points are obtained as ξ_o changing from 0.2 to 0.8, and the corresponding values of (ξ_o, γ, χ) are listed in Table I. Sahin *et al.*[5] demonstrated that the 24th harmonic is more sensitive to harder samples and the 8th harmonic is more sensitive to softer samples when monitoring the cantilever deflection at the harmonic corresponding to the third mode. Therefore, the choice of the appropriate higher harmonic is determined by the material properties.

TABLE I. Values of (ξ_o, γ, χ) which yield integer numbers for both ω_2/ω_1 and ω_3/ω_1.

ω_2/ω_1	ω_3/ω_1	ξ_o	γ	χ	ω_2/ω_1	ω_3/ω_1	ξ_o	γ	χ	ω_2/ω_1	ω_3/ω_1	ξ_o	γ	χ
3	8	0.50	0.22	0.04	5	11	0.30	0.28	0.14	7	21	0.60	1.24	1.87
3	8	0.70	0.22	0.04	5	12	0.30	0.41	0.22	7	21	0.70	1.38	2.62
3	9	0.50	0.28	0.08	5	12	0.70	0.58	0.23	8	23	0.30	1.66	2.28
4	9	0.40	0.26	0.07	5	14	0.40	0.74	0.44	8	24	0.40	1.96	2.04
4	9	0.70	0.26	0.08	5	14	0.50	0.72	0.46	8	24	0.70	2.16	2.82
4	10	0.40	0.35	0.13	7	20	0.30	1.34	1.46	8	25	0.50	1.54	2.72
4	11	0.60	0.45	0.20	7	20	0.40	1.30	1.39	8	25	0.60	1.85	2.75

The normal modes are characterized by the effective stiffness, natural frequency and quality factor.[36] The presence of the damping reduces the natural frequencies. Compared with that of the fundamental mode, the force constant of $k_n = m\omega_n^2$ (ω_n: natural frequency of the nth mode) is larger in higher mode. As a result, the damping influence on higher modes is smaller. The falling amplitude of the higher natural frequency is smaller than that of the fundamental frequency. Therefore, as shown in Fig. 3, the ratios of ω_2/ω_1 and ω_3/ω_1 are higher than those of the undamped step-like cantilever with the giving ξ_o, γ and χ. In fact, the vibration of AFM in air is with small damping.[37] The shift of natural frequency due to small damping can be ignored in air or vacuum.[38] The variation tendency for the case of ω_3/ω_1 is even smaller.

In summary, a step-like cantilever, whose natural frequency of the second mode or third mode is an integer multiple of the fundamental frequency, is proposed to enhance the signals of the higher harmonics. Besides, the first three natural frequencies can be simultaneously excited with proper step-like cantilever geometric parameters. Therefore, the information of the material properties can be extracted from the enhanced higher harmonic signals. By this way, the step-like cantilever can simultaneously sense the topography and mechanical properties with the increased spatio-temporal resolution. In the step-like cantilever, the ratio of ω_2/ω_1 shows a minimum when both parts are with the same length. For a step-like cantilever is with a large difference in the length of the two parts, the bending of the thinner part dominates, and the natural frequencies are close to those of a uniform cantilever.

See supplementary material for the detailed computational procedures of the natural frequencies of the step-like cantilever, and the detailed proof that the figure with length ratio ξ_o and figure with length ratio $1 - \xi_o$ are symmetrical to the straight line of $\chi = \gamma$.

This work was supported by the National Natural Science Foundation of China (NSFC No. 11772335).

[1] E. Hacker and O. Gottlieb, Appl. Phys. Lett. **101**, 053106 (2012).
[2] M. Stark, R. W. Stark, W. M. Heckl, and R. Guckenberger, Appl. Phys. Lett. **77**, 3293 (2000).
[3] O. Sahin and A. Atalar, Appl. Phys. Lett. **79**, 4455 (2001).
[4] N. F. Martínez, J. R. Lozano, E. T. Herruzo, F. García, C. Richter, T. Sulzbach, and R. García, Nanotechnology **19**, 384011 (2008).
[5] O. Sahin, C. F. Quate, O. Solgaard, and A. Atalar, Phys. Rev. B **69**, 165416 (2004).
[6] S. Hembacher, F. J. Giessibl, and J. Mannhart, Science **305**, 380 (2004).
[7] S. Crittenden, A. Raman, and R. Reifenberger, Phys. Rev. B **72**, 235422 (2005).
[8] M. Balantekin and A. Atalar, Phys. Rev. B **71**, 125416 (2005).
[9] C. A. Amo, A. P. Perrino, A. F. Payam, and R. García, ACS Nano **11**, 8650 (2017).
[10] D. Ebeling, B. Eslami, and S. D. J. Solares, ACS Nano **7**, 10387 (2013).
[11] R. Hillenbrand, M. Stark, and R. Guckenberger, Appl. Phys. Lett. **76**, 3478 (2000).
[12] O. Sahin, G. Yaralioglu, R. Grow, S. F. Zappe, A. Atalar, C. F. Quate, and O. Solgaard, Sens. Actuators, A **114**, 183 (2004).
[13] T. R. Rodríguez and R. García, Appl. Phys. Lett. **80**, 1646 (2002).
[14] T. R. Rodríguez and R. García, Appl. Phys. Lett. **84**, 449 (2004).
[15] M. Balantekin and A. Atalar, Appl. Phys. Lett. **87**, 243513 (2005).
[16] O. Sahin, S. Magonov, C. Su, C. F. Quate, and O. Solgaard, Nat. Nanotechnol. **2**, 507 (2007).
[17] J. R. Felts and W. P. King, J. Micromech. Microeng. **19**, 115008 (2009).
[18] M. Loganathan and D. A. Bristow, Rev. Sci. Instrum. **85**, 043703 (2014).
[19] B. Jeong, C. Pettit, S. Dharmasena, H. Keum, J. Lee, J. Kim, S. Kim, D. M. McFarland, L. A. Bergman, A. F. Vakakis, and H. Cho, Nanotechnology **27**, 125501 (2016).
[20] A. Schuh, M. Hofer, T. Ivanov, and I. W. Rangelow, J. Microelectromech. Syst. **24**, 1622 (2015).
[21] B. Zhu, S. Zimmermann, X. Zhang, and S. Fatikow, J. Mech. Design **139**, 012303 (2016).
[22] W. Zhang, Y. Chen, and J. Chu, Rev. Sci. Instrum. **88**, 106101 (2017).
[23] W. Zhang, Y. Chen, and J. Chu, Sens. Actuators, A **255**, 54 (2017).
[24] H. Li, Y. Chen, and L. Dai, Appl. Phys. Lett. **92**, 151903 (2008).
[25] S. Sadewasser, G. Villanueva, and J. A. Plaza, Appl. Phys. Lett. **89**, 033106 (2006).
[26] J. Cai, Q. Xia, Y. Luo, L. Zhang, and M. Y. Wang, Appl. Phys. Lett. **106**, 071901 (2015).
[27] D. K. Parsediya, J. Singh, and P. K. Kankar, J. Mech. Sci. Technol. **29**, 4823 (2015).
[28] S. Sadewasser, G. Villanueva, and J. A. Plaza, Rev. Sci. Instrum. **77**, 073703 (2006).
[29] A. Keyvani, H. Sadeghian, M. S. Tamer, J. F. L. Goosen, and F. van Keulen, J. Appl. Phys. **121**, 244505 (2017).
[30] J. Cai, M. Y. Wang, and L. Zhang, Rev. Sci. Instrum. **86**, 125007 (2015).
[31] J. Cai, M. Y. Wang, Q. Xia, and Y. Luo, Eng. Opt. **49**, 43 (2016).
[32] Z. Li, T. Shi, and Q. Xia, Microsyst. Technol. (2017).
[33] Y. Zhang and K. D. Murphy, J. Sound. Vib. **330**, 5569 (2011).

[34] Y. Zhang, H. Zhao, and L. Zuo, J. Sound. Vib. **331**, 5141 (2012).
[35] Z. Zheng, R. Xu, and Z. Cheng, Sci. China. Technol. Sc. **46**, 437 (2016).
[36] R. García and E. T. Herruzo, Nat. Nanotechnol. **7**, 217 (2012).
[37] S. Rützel, S. I. Lee, and A. Raman, Proc. R. Soc. A **459**, 1925 (2003).
[38] Y. Zhang, Sens. Actuators, A **194**, 169 (2013).